Micromagnetics Simulation of High Energy Density Permanent Magnets

Dieter Süss, Thomas Schrefl, and Josef Fidler

***Abstract*—A finite element approach is used to calculate the influence of different grain boundary phases on the reversal process of sintered Nd–Fe–B magnets. To calculate equilibrium states of the magnetic polarization the total Gibbs' free energy is minimized with a quasi-Newton conjugate gradient method. It was found that the grain boundary phases influence the coercive field significantly. For a perfect microstructure the numerical results agree well with the Stoner–Wohlfarth theory. A reduction of the magnetocrystalline anisotropy near grain boundaries leads to a linear decrease of the coercive field. In contrast to the Stoner–Wohlfarth theory the coercive field will decrease with increasing alignment of the easy axies if the anisotropy is reduced near grain boundaries. The finite element simulations confirm the experimental results that nonmagnetic Nd-rich phases at grain boundary junctions significantly increase the coercive field.**

***Index Terms*—Finite element method, grain boundary phases, NdFeB-magnets, numerical micromagnetics.**

I. Introduction

HIGH energy density magnets exhibit a complex microstructure which is strongly influenced by the processing technique. High performance Nd–Fe–B magnets ($BH_{\max} > 400$ kJ/m^3) are produced by sintering, which leads to grain sizes above 1 μm. Besides the hard magnetic $Nd_2Fe_{14}B$ phase Nd–Fe–B magnets contain at least five more phases [1]. These additional phases strongly influence the coercivity. This can be seen in the discrepancy between the theoretical coercive fields obtained from the Stoner–Wohlfarth theory [2] of $Nd_2Fe_{14}B$ magnets and measured coercive fields. Intergranular phases may change the coupling behavior of the hard magnetic grains. Distorted grain boundary phases with a reduced magnetocrystalline anisotropy favor the formation of reversed domains. The composition of these phases can be influenced by substituent and dopant elements [3], [4]. Numerical micromagnetic modeling is an effective tool to analyze the influence of intergranular phases on the reversal process. Due to the large grain sizes of sintered magnets only 2-D or axisymmetric finite element simulations were performed up to now [5], [6]. We use a three dimensional approach which is restricted to a representative part of the microstructure. We simulate the reversal process in a region near the junction of four grains.

Manuscript received February 14, 2000. This work was supported by the Austrian Science Fund (Project 13433-PHY and Y132-PHY).

The authors are with the Institute of Applied and Technical Physics, Vienna University of Technology, Wiedner Hauptstr. 8-10, A-1040 Vienna, Austria (e-mail: {suess; thomas.schrefl}@tuwien.ac.at; fidler@email.tuwien.ac.at).

Publisher Item Identifier S 0018-9464(00)08243-1.

II. Micromagnetic Background

To calculate the hysteresis loop the total Gibbs' free energy is subsequently minimized for different external fields. In the micromagnetic approach the total Gibbs' free energy can be expressed as the sum of the exchange energy, the magnetocrystalline anisotropy energy, the magnetostatic energy, and the Zeeman energy [7]:

$$E_t = \int \left[\frac{A}{J_s^2} \sum_{i=1}^{3} (\nabla J_i)^2 + f_k(\boldsymbol{J}) - \tfrac{1}{2} \boldsymbol{J} \cdot \boldsymbol{H}_d - \boldsymbol{J} \cdot \boldsymbol{H}_{ext} \right] dV \tag{1}$$

where $\boldsymbol{J}$ denotes the magnetic polarization. A is the exchange constant and f_k the magnetocrystalline anisotropy energy density, which can be written for the uniaxial case as $f_k(\boldsymbol{J}) = -K_1(\boldsymbol{u} \cdot \boldsymbol{J}/J_s)^2$. $\boldsymbol{H}_d$ and $\boldsymbol{H}_{ext}$ denote the demagnetizing and the external field, respectively. $\boldsymbol{u}$ is the unit vector parallel to the uniaxial easy axis. For the evaluation of equation (1) the finite element method is used. The magnetic particle is subdivided into finite elements. The magnetic polarization is defined on each node of the finite element mesh. Using piecewise polynomial shape functions the magnetization can be evaluated within each finite element. We use a hybrid finite element/boundary integral method for computing the demagnetizing field. The advantage of this method is that no elements outside the magnetic particle are needed, to consider the boundary conditions of the stray field problem at infinity.

The total Gibbs' free energy has to be minimized under the constraint that $|\boldsymbol{J}|$ is constant. Convergence problems were reported when a Newton method is used for the minimization of the energy together with a Lagrange-multiplier approach to realize $|\boldsymbol{J}| = J_s$ [8]. The constraint $|\boldsymbol{J}| = J_s$ can be easily satisfied using polar coordinates for the magnetic polarization at node i, such that $J_{x,i} = J_s \sin\theta_i \cos\varphi_i$, $J_{y,i} = J_s \sin\theta_i \sin\varphi_i$ and $J_{z,i} = J_s \cos\theta_i$. Hence the amount of variables will be reduced to $2N$, if N denotes the number of nodes. We use a preconditioned, limited memory quasi-Newton conjugate gradient method [9] for minimizing the total Gibbs' energy. Conjugate gradient based minimization techniques requires only the energy and the gradient of the energy to search the local minima. For V_i approaching zero the gradient of the energy at the nodal point i can be expressed as

$$\frac{\partial E_t}{\partial \theta_i} = \int \sum_{k=x,\,y,\,z} \frac{\partial E_t}{\partial J_{k,i}} \frac{\partial J_{k,i}}{\partial \theta_i} \, dV = -V_i \boldsymbol{H}_{\text{eff},i} \frac{\partial \boldsymbol{J}_i}{\partial \theta_i}, \tag{2}$$

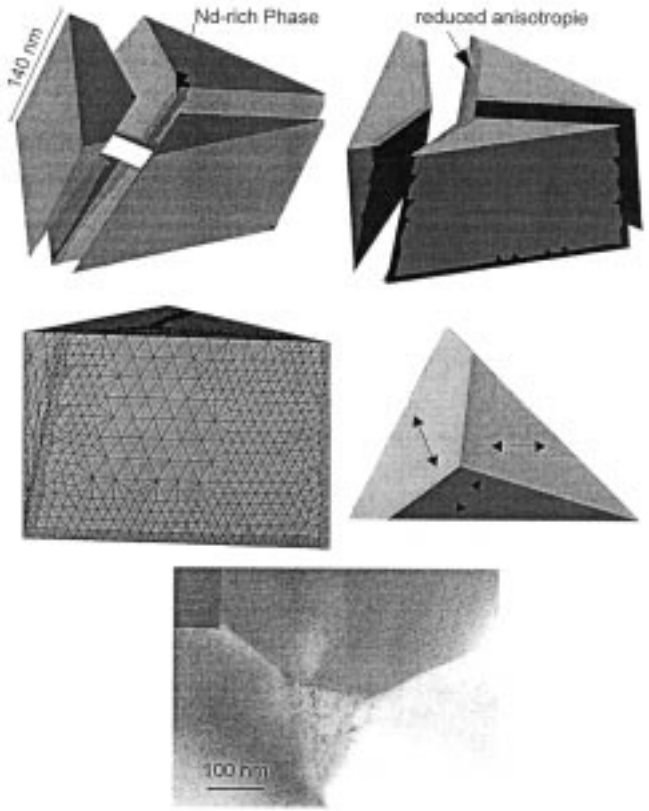

Fig. 1. The upper images show the microstructur for the finite element model. In the dark regions the intrinsic properties are varied. The picture at the bottom shows a TEM micrograph of a Nd–Fe–B sintered magnet.

$$\frac{\partial E_t}{\partial \varphi_i} = \int \sum_{k=x,\,y,\,z} \frac{\partial E_t}{\partial J_{k,\,i}} \frac{\partial J_{k,\,i}}{\partial \varphi_i}\, dV = -V_i \boldsymbol{H}_{\mathrm{eff},\,i} \frac{\partial \boldsymbol{J}_i}{\partial \varphi_i}. \quad (3)$$

$\boldsymbol{H}_{\mathrm{eff},i}$ denotes the effective field, which is the negative functional derivative of the total Gibbs' energy, at node i.

V_i denotes the volume surrounding the nodal point i, such that

$$\sum_i V_i = V \quad \text{and} \quad V_i \cap V_j = 0 \qquad \text{for } i \neq j. \quad (4)$$

Within the framework of finite elements the effective field can be approximated

$$\boldsymbol{H}_{\mathrm{eff,\,i}} = -\left(\frac{\delta E_t}{\delta \boldsymbol{J}}\right)_i = \frac{1}{V_i}\frac{\partial E_t}{\partial \boldsymbol{J}_i}, \qquad \text{for } V_i \to 0. \quad (5)$$

III. Influence of Intergranular Phases on Coercivity

Our micromagnetic model is based on TEM investigations of Nd–Fe–B magnets. The TEM micrograph of Fig. 1 shows the grain junction of three grains and a small amount of Nd-rich phase (the triangular area in the middle of the picture). The upper images of Fig. 1 show the corresponding model of the microstructure which is used for the simulations. The four grains are separated for a better visibility. The dark regions of the upper left picture show the dispersion of Nd-rich phases. The anisotropy constant is varied in the regions which are drawn dark in the upper right picture of Fig. 1. The arrows in the middle right picture of Fig. 1 represent the projection of the easy axis onto the image plane.

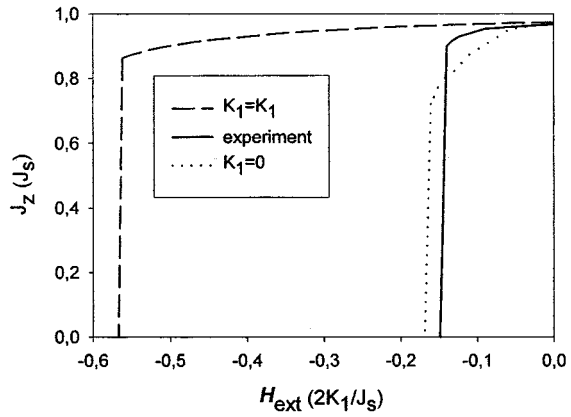

Fig. 2. Comparison of the demagnetizing curves of magnets with perfect grain boundaries and distorted grain boundaries with experimental data.

The required computational time limits the number of finite elements. Thus only a representative part of the Nd–Fe–B magnets can be simulated. The typical domain wall width of the material determines the upper limit for the size of the finite elements, at least in regions where domain walls occur. The nucleation of reversed domains are expected near grain boundary junctions. Hence we use a coarse mesh in regions near the center of a hard magnetic grain and a fine mesh near grain boundary junctions. The mesh is shown in the middle left picture of Fig. 1. The number of finite elements is about 40 000. For the calculations the material parameters of the $Nd_2Fe_{14}B$ phase at $T = 300$ K has been taken from Sagawa *et al.* [10] ($K_1 = 4,\,5\ 10^6$ J/m^3, $J_s = 1,\,61$ T, $A = 12,\,5\ 10^{-12}$ J/m).

For a perfect microstructure the calculated coercive fields agree well with the Stoner–Wohlfarth theory. The most misoriented grain, which has the largest angle between the easy axis and the alignment direction, determines the coercive field. The coercive field decreases with increasing misalignment. The values of the calculated coercive field are about 6% smaller than the values predicted by the Stoner–Wohlfarth theory.

More realistic micromagnetic simulations have to consider the complex multiphase microstructure of Nd–Fe–B magnets [1]. To estimate the thickness of the inhomogeneous intergranular phase Kronmüller *et al.* [11] compared the temperature dependence of the coercivity of an analytical model with experimental data. For sintered magnets the predicted thickness varies between 1 and 3 nm. In order to obtain realistic values of the coercive field in the simulation the anisotropy constant is reduced to zero in a 7 nm thick region near the grain boundaries, as shown in the upper right picture of Fig. 1. This defect in the magnetocrystalline anisotropy decreases the coercive field from 3200 kA/m to 900 kA/m. Fig. 2 shows the corresponding demagnetizing curves together with the experimental demagnetizing curve of a high-energy magnet with low oxygen content.

The calculated demagnetizing curve of the magnet with distorted grain boundaries has little squareness. The reason is the

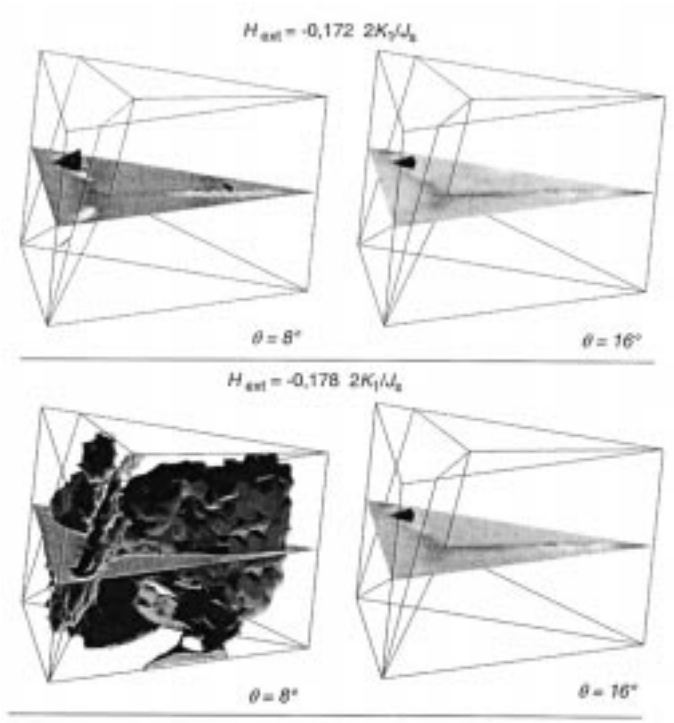

Fig. 3. The isosurfaces represent the regions where $J_z/J_s < 0,7$. In these regions the nucleation of reversed domains will start.

high volume of reduced anisotropy, since only a part of the magnet is simulated.

In order to investigate the nucleation process which occurs within the magnet we subtract the demagnetizing field of the saturated particle from the stray field. As a consequence shape effects, which lead to high strayfield near corners are reduced. The reduction of the magnetocrystalline anisotropy reverses the dependence of the coercive field on the degree of alignment. Bachmann *et al.* [12] observed a similar behavior of the coercivity on the degree of alignment for nanocrystalline magnets. The coercive field increases by about 80 kA/m as the misalignment angle is changed from 8° to 16°. Fig. 3 compares the nucleation process for two different degrees of alignment. The isosurfaces represent the reversed nucleus. In the well aligned sample (the two left images of Fig. 3) higher demagnetizing field initiates the nucleation of reversed domains in the defect region. The simulations are in agreement with experimental data which show a slight increase of coercivity with misalignment for Dy-free Nd–Fe–B magnets, whereas a decrease of the coercive field with increasing misalignment is observed in highly coercive, Dy-containing Nd–Fe–B magnets [13].

The coercive field of Nd–Fe–B sintered magnet increases with increasing Nd content [14]. For the simulations a Nd-rich phase at the grain boundary junction of three grains is assumed as shown in the upper left picture of Fig. 1. The diameter of this phase, where the exchange constant and the spontaneous magnetic polarization are set to be zero, is about 7 nm. The comparison of the demagnetizing curves of Fig. 4 shows that the coercive field increases by about 15% as non magnetic Nd-rich phases near grain boundary junctions are taken into account. The simulations show that the presence of the Nd-rich phase

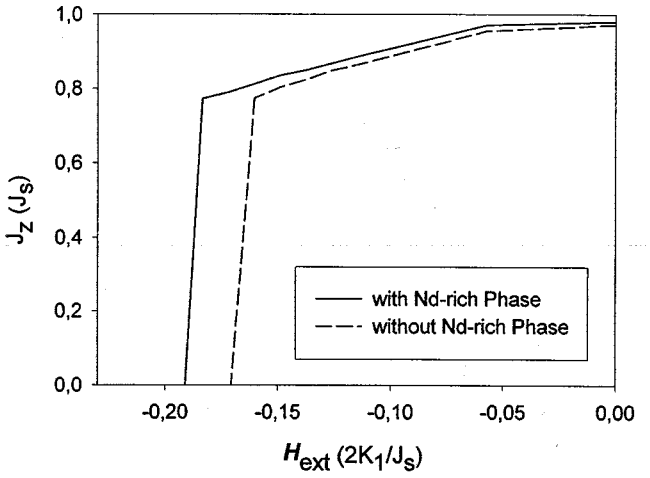

Fig. 4. Effect of Nd-rich phases near grain boundary junction on the demagnetizing process.

significantly changes the exchange and the magnetostatic interactions. As a consequence the nucleation of reversed domains is suppressed.

REFERENCES

[1] J. Fidler and K. G. Knoch, "Electron microscopy of Nd–Fe–B based magnets," *J. Magn. Magn. Mater.*, vol. 80, pp. 48–56, 1989.
[2] E. C. Stoner and E. P. Wohlfarth, "A mechanism of magnetic hystersis in heterogeneous alloys," *Philos. Trans. R. Soc.*, vol. 240, pp. 599–642, 1948.
[3] J. Bernardi, J. Fidler, and F. Födermayr, "The effect of V or W additives to microstructure and coercivity of Nd–Fe–B based magnets," *IEEE Trans. Magn.*, vol. 28, pp. 2127–1129, 1992.
[4] J. Fidler, "Rare earth intermetallic magnets," in *Inst. Phys. Conf. Ser. no. 152, Section G: Magnetic Materials*, 1998, pp. 805–813.
[5] T. Schrefl, H. F. Schmidts, J. Fidler, and H. Kronmüller, "Nucleation fields and grain boundaries in hard magnetic materials," *IEEE Trans. Magn.*, vol. 29, pp. 2878–2880, 1993.
[6] J. C. Toussaint, B. Kevorkian, D. Givord, and M. F. Rossignol, "Micromagnetic modeling of magnetization reversal in permanent magnets," in *Proc. 9th Int. Symp. Magnetic Anisotropy and Coercivity in Rare-Earth Transition Metal Alloys*. Singapore: World Scientific, 1996, pp. 59–68.
[7] W. F. Brown Jr., *Micromagnetics*. New York: Wiley, 1963.
[8] A. Viallix, F. Boileau, R. Klein, and J. J. Niez, "A new method for finite element calculation of micromagnetics problems," *IEEE Trans. Magn.*, vol. 24, pp. 2371–2373, 1988.
[9] P. E. Gill, W. Murray, and M. H. Wright, *Practical Optimization*. London/New York/Toronto: Academic, 1981.
[10] M. Sagawa, S. Fujimura, H. Yamamoto, Y. Matsuura, and S. Hirosawa, "Magnetic properties of rare-earth-iron–boron permanent magnet materials," *J. Appl. Phys.*, vol. 57, pp. 4094–4096, 1985.
[11] H. Kronmüller, K. D. Durst, and M. Sagawa, "Analysis of the magnetic hardening mechanism in Re–Fe–B permanent magnets," *J. Magn. Magn.*.
[12] M. Bachmann, R. Fischer, and H. Kronmüller, "Simulation of magnetization process in real microstructures," in *10th Int. Symposium on Magnetic Anisotropy and Coercivity in Rare-Earth Transition Metal Alloys*, L. Schultz and K.-H. Müller, Eds. Dresden: Werkstoff-Informationsgesellschaft, 1998, pp. 217–236.
[13] A. S. Kim, F. E. Camp, and H. H. Stadelmaier, "Relation of remanence and coercivity of Nd,(Dy)–Fe,(Co)–B sintered permanent magnets to crystallite orientation," *J. Appl. Phys.*, vol. 76, no. 10, pp. 6265–6267, 1994.
[14] S. Hirosawa and Y. Kaneko, "Rare earth magnets with high energy products," in *Proc. 15th Int. Workshop on Rare-Earth Magnets and their Applicat.*, Dresden, Germany, 1998, p. 43.